Adaptive Current-Mode Control of a High Step-Up DC–DC Converter

Chok-You Chan, Satyajit Hemant Chincholkar, and Wentao Jiang

***Abstract*—A new adaptive current-mode control of a high step-up dc–dc converter is presented. The converter gives a very high voltage gain without using a transformer and maintains low voltage stress across the power devices. The adaptive controller is formed by combining the existing current-mode control law and an adaptive law that generates the inverse of the load resistance. The structure of the proposed adaptive law is such that the derivative of the estimate is both optimized and bounded. To facilitate the controller design, the derived averaged state-space model of the converter with parasitic elements is used. An approximate stability analysis is carried out to gain some insight into the behavior of the adaptive-controlled system. Some experimental results comparing the performance of the proposed adaptive current-mode controller with that of the existing current-mode controller are also presented.**

***Index Terms*—Adaptive control, current-mode control, high step-up dc–dc converter.**

I. Introduction

THE mass usage of various nonrenewable energy resources such as coal, petroleum has led to several environmental concerns like air pollution, global warming, and green-house effect [1]–[3]. Also, considering the growing energy demands of the present society, it is necessary to give some attention to the development of clean and renewable energy resources such as wind energy, fuel cells, photovoltaics (PVs) to replace the traditional nonrenewable sources of energy [2], [4]. However, the output voltages produced by these renewable energy resources are very low and not easily compatible with an electric grid. Also, the output voltage varies with several external parameters such as solar insolation on the PV array. To overcome these problems, a dc–dc converter with a sufficient amount of gain is usually employed before interfacing with the grid [5], [6]. The dc–dc converter not only increases the output voltage of the renewable energy resources but also provides the necessary control action against load and line variations.

The gain of the conventional dc–dc boost converter is limited to approximately six times its input voltage due to practical considerations [6], [7]. To obtain a high gain, it needs to operate at some extremely high values of the duty ratio. This may lead to a severe reverse recovery problem of the diode and little room for control when dealing with load and line disturbances [6], [7]. To overcome these problems, several high step-up dc–dc converter topologies have been reported in the past few years. These topologies can be broadly classified into two types, viz., the isolated and nonisolated topologies [6]–[15]. However, if an industrial application does not require any electrical isolation, the use of a transformer-based dc–dc converter would only increase the overall size and cost of the system. In addition, the leakage inductor energy of the transformer could degrade the overall efficiency of the converter and may also lead to high voltage stress across the switching devices [1], [7], [13]. This makes transformerless topologies a more interesting choice. Among these, a high step-up dc–dc converter can be an attractive solution that has several advantages [6]. It maintains a low voltage stress across its diodes, which allow the use of Schottkey rectifiers for reducing the reverse-recovery current problem. Also, this converter requires a lower voltage rated MOSFET switch, which improves the efficiency of the converter by reducing the switching and conduction losses. Despite such various advantages offered by this converter, there is a scarcity of works addressing its regulation problem. To bridge this gap, a new adaptive current-mode control of the high step-up dc–dc converter is presented in this paper. To better appreciate the significance of the proposed controller, a brief overview of some past works done in the area of control of high-order dc–dc boost converters is presented.

The voltage-mode control and current-mode control are two widely used methodologies for regulating the output voltage in dc–dc converters. However, considering the nonminimum phase nature of the control-to-output transfer function of the boost-type dc–dc converters, it is difficult to design their voltage-mode control using a single voltage loop. To overcome this problem, an indirect approach of control in which the output voltage of the converter can be regulated via the inductor current control was employed in [16]–[19]. However, the structures of the controllers used in [16]–[19] are such that they need a constant reference inductor current term to compute the control signal. This term, in turn, depends on the load resistance R of the converter. For implementation purposes, the value of R is assumed to be constant so that the reference inductor current can be calculated. However, in practical systems, R could vary. Also, when R is unknown, it is impossible to calculate the value of the reference inductor current. These are the major drawbacks of the traditional current-mode controller.

Manuscript received May 20, 2016; revised July 20, 2016 and October 10, 2016; accepted November 6, 2016. Date of publication November 15, 2016; date of current version April 24, 2017. Recommended for publication by Associate Editor P. S. Shenoy.

The authors are with the School of Electrical and Electronic Engineering, Nanyang Technological University, Singapore 639798 (e-mail: ecychan@ntu.edu.sg; saty0007@e.ntu.edu.sg; wjiang003@e.ntu.edu.sg).

Color versions of one or more of the figures in this paper are available online at http://ieeexplore.ieee.org.

Digital Object Identifier 10.1109/TPEL.2016.2628780

Various other indirect control methodologies have also been used to regulate the output voltage in high-order dc–dc converters. Among them, a widely used hysteresis modulation (HM) based indirect sliding-mode controller (SMC) has several advantages such as ease of implementation and reduced risk of saturation while operating at high values of the duty cycle [13], [20]. However, this solution uses a variable switching frequency, which may lead to inductor and switching losses as well as electromagnetic-interference generation [21]. If a pulse width modulation (PWM) based SMC is employed, a double integral of the output voltage error is required to reduce the steady-state output error to a negligible value [22]. This increases the computations and complexity of the controller implementation [23]. In summary, the question of how to choose a suitable indirect current-mode controller for high-order boost-type dc–dc converters is still an open problem and some further investigations are required to address this issue.

In this paper, a new adaptive current-mode controller for the regulation of the high step-up dc–dc converter of [6] is proposed. In order to overcome the drawbacks of the conventional current-mode controller [16]–[19] in handling unknown loads, the proposed controller uses the estimate of the inverse of the load resistance to calculate the reference inductor current of the converter. This estimate, namely, $\hat{\theta}$ is obtained from an appropriate adaptation algorithm. The proposed adaptation algorithm, which is given in the normalized form, leads to an optimized $d\hat{\theta}/dt$. Moreover, in contrast to existing adaptive schemes [24], the proposed adaptation algorithm offers more tuning parameters, which can bring about a more satisfactory response since $d\hat{\theta}/dt$ is bounded by a user specified constant. Also, since it is estimating the load resistance, the adaptive controller is expected to be highly responsive to a change of load as compared to the traditional current-mode controller. This is borne out by the experimental results comparing the performance of the proposed controller with that of the traditional current-mode controller.

II. Modeling of the High Step-Up DC–DC Converter

Fig. 1 shows the circuit of the high step-up dc–dc converter with some parasitic resistances. Assuming that the converter is operating in the continuous conduction mode, the circuit operation can be divided into two stages, namely, "stage 1" of operation when switch "S" is "off" [see Fig. 1(b)] and "stage 2" of operation when switch "S" is "'on" [see Fig. 1(c)]. In Fig. 1, r_C, r_{C_1}, and r_{C_2} represent the parasitic resistances of the capacitors C, C_1, and C_2, respectively. It should be noted that, without considering these parasitic resistances, it is not possible to obtain the derivatives of v_C, v_{C_1}, and v_o in terms of the state variables i_{L_1}, v_C, v_{C_1}, and v_o in "stage 2," i.e., it is not possible to obtain the averaged state-space model of the converter.

A. Averaged State-Space Model

To obtain the averaged state-space model of the converter, it has been assumed that the inductors L_1 and L_2 have the same value ($L_1 = L_2$) and capacitors C_1 and C_2 have the same value and equal parasitic resistance value ($C_1 = C_2$ and $r_{C_1} = r_{C_2}$).

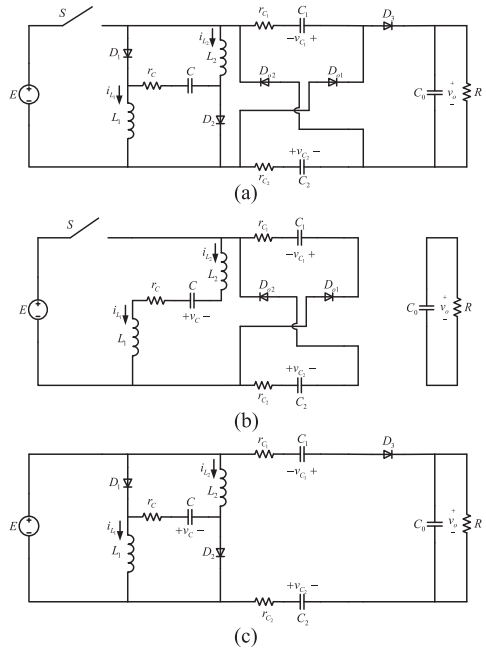

Fig. 1. High step-up dc–dc converter and its operating modes: (a) circuit diagram; (b) "Stage 1" of operation when switch "S" is "off"; and (c) "Stage 2" of operation when switch "S" is "on."

Stage 1: During this stage of operation, switch "S" is turned "off" [Fig. 1(b)] and two diodes D_{o1} and D_{o2} are forward biased. This provides a path for the inductor currents i_{L_1} and i_{L_2} to flow, and the energy stored in inductors L_1 and L_2 is transferred to the capacitors C_1 and C_2 to charge them. On the other hand, the capacitor C_0 is discharged to provide the energy to load R. Since the inductor currents flowing through the two inductors L_1 and L_2 are the same (i.e., $i_{L_1} = i_{L_2}$), their dynamics can be represented by the same differential equation. Similarly, the two capacitors C_1 and C_2 are effectively in parallel and thus the dynamics of v_{C_1} and v_{C_2} can be combined to form a single differential equation. The differential equations for this stage of operation are given by

$$\dot{x} = A_1 x + B_1 E \tag{1}$$

where $x = [\, i_{L_1} \;\; v_C \;\; v_{C_1} \;\; v_o \,]$ and

$$A_1 = \begin{bmatrix} -\frac{\beta}{2L_1} & \frac{1}{2L_1} & -\frac{1}{2L_1} & 0 \\ -\frac{1}{C} & 0 & 0 & 0 \\ \frac{1}{2C_1} & 0 & 0 & 0 \\ 0 & 0 & 0 & -\frac{1}{RC_o} \end{bmatrix}, \quad B_1 = \begin{bmatrix} 0 \; 0 \; 0 \; 0 \end{bmatrix}^T, \text{ and}$$

$\beta = r_C + r_{C_1}/2.$

Stage 2: In this stage, switch "S" is turned "on" and the equivalent circuit diagram is shown in Fig. 1(c). The input voltage E is charging the capacitor C, whereas the two capacitors C_1 and C_2 provide the energy to load. The differential equations representing this stage of operation can be written as

$$\dot{x} = A_2 x + B_2 E \tag{2}$$

where matrices A_2 and B_2 are given by

$$A_2 = \begin{bmatrix} 0 & 0 & 0 & 0 \\ 0 & -\frac{1}{r_C C} & 0 & 0 \\ 0 & 0 & -\frac{1}{r_{C_1} C_1} & \frac{1}{2r_{C_1} C_1} \\ 0 & 0 & \frac{1}{r_{C_1} C_o} & -\left(\frac{1}{RC_o} + \frac{1}{2r_{C_1} C_o}\right) \end{bmatrix} \text{ and}$$

$$B_2 = \begin{bmatrix} \frac{1}{L_1} & \frac{1}{r_C C} & -\frac{1}{2r_{C_1} C_1} & \frac{1}{2r_{C_1} C_o} \end{bmatrix}^T.$$

Applying the generalized state-space averaging technique [15] to (1) and (2) yields the following generalized averaged state-space model of the converter given by

$$\dot{x} = (A_1 u' + A_2 u)\, x + (B_1 u' + B_2 u)\, E \tag{3}$$

where u denotes the control signal of switch "S" such that $u \in (0, 1)$ and $u' = 1 - u$.

B. Equilibrium Values

By setting (3) to zero, the following equilibrium values are obtained:

$$\begin{aligned} I_{L_1} &= \frac{2EU\,(U+3)}{(1-U)\,(-RU^2 + RU + 4r_C + 2r_{C_1})}, \\ V_C &= \frac{E\left(2r_{C_1} - 2r_c + RU - 2r_c U - RU^2\right)}{(-RU^2 + RU + 4r_C + 2r_{C_1})}, \\ V_{C_1} &= \frac{E\left(2r_{C_1} - 2r_c + RU + r_{C_1} U + RU^2\right)}{(-RU^2 + RU + 4r_C + 2r_{C_1})}, \\ V_o &= \frac{ERU\,(U+3)}{(-RU^2 + RU + 4r_C + 2r_{C_1})} \end{aligned} \tag{4}$$

where U, I_{L_1}, V_C, V_{C_1}, and V_0 represent the equilibrium values of u, i_{L_1}, v_C, v_{C_1}, and v_o, respectively. A simplification of the expressions of the equilibrium values can be done if it is assumed that $r_C/R \approx 0$ and $r_{C_1}/R \approx 0$. Thus, from the expression of V_o in (4), setting V_o at the desired value V_d, the approximate value of U can be written as

$$U_a = \frac{V_d - 3E}{V_d + E} \tag{5}$$

Using (5) in (4), and using $r_C/R \approx 0$ and $r_{C_1}/R \approx 0$ give

$$I_{L_{1a}} = \frac{V_d\,(V_d + E)}{2RE}, \quad V_{Ca} = E, \quad V_{C_{1a}} = \frac{V_d - E}{2} \tag{6}$$

where $I_{L_{1a}}$, V_{Ca}, and $V_{C_{1a}}$ are the approximate values of I_{L_1}, V_C, and V_{C_1}, respectively.

C. Model Validation Using Frequency-Domain Technique

First, to verify the accuracy of the averaged state-space model of the converter using the frequency-domain technique, a small-signal linearized model was derived (refer to Appendix). The Bode diagram obtained from the resulting control-to-output transfer function was compared to the Bode diagram obtained from the actual converter circuit implemented in PSIM software,

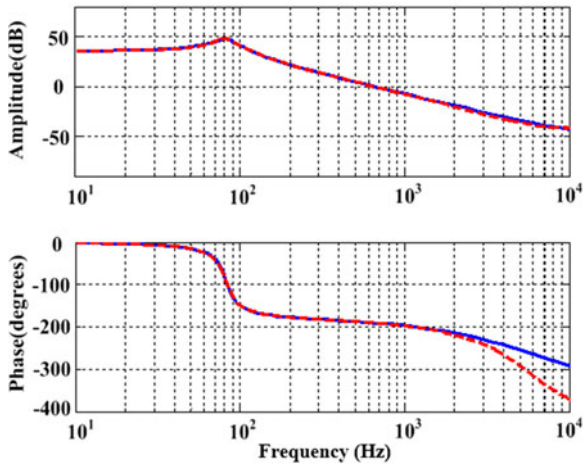

Fig. 2. Bode plot of the control-to-output transfer function of the converter $(\tilde{v}_0(s)/\tilde{u}(s))$ (solid line: Bode plot obtained from the transfer function (8), dotted line: Bode plot obtained from the actual open-loop converter circuit implemented in PSIM software).

version 9.0.3. The following circuit parameter values were used:

$$\begin{aligned} E &= 3.3\,\text{V}, \quad V_d = 25\,\text{V}, \quad L_1 = L_2 = 1\,\text{mH}, \\ C &= C_1 = C_2 = C_0 = 68\,\mu\text{F}, \quad R = 1\,\text{k}\Omega, \\ r_C &= r_{C_1} = r_{C_2} = 0.5\,\Omega, \quad F_s = 50\,\text{kHz} \end{aligned} \tag{7}$$

where F_s is the converter switching frequency. The corresponding control signal-to-output voltage transfer function $\tilde{v}_0(s)/\tilde{u}(s)$ is given by

$$G(s) = \frac{\tilde{v}_0(s)}{\tilde{u}(s)} = \frac{-3.0924 \times 10^7 \left(s - 3.078 \times 10^4\right)\left(s + 3.923 \times 10^4\right)}{\left(s + 5.884 \times 10^4\right)\left(s + 3.919 \times 10^4\right) \times \left(s^2 + 129.7s + 2.682 \times 10^4\right)} \tag{8}$$

where the superscript "$\sim$" represents the small signal variations in the steady-state values such that $v_o = V_d + \tilde{v}_0$ and $u = U_a + \tilde{u}$. In Fig. 2, the curves in solid line are obtained from the transfer function (8), whereas the curves in dotted line are obtained from the actual converter circuit implemented in PSIM software. A good correspondence between the analytical Bode plot obtained using the state-space model of the converter and the Bode plot obtained using the actual open-loop converter circuit validates the accuracy of the averaged state-space model of the converter at intermediate frequencies.

D. Model Validation Using Time-Domain Technique

Next, in order to verify the accuracy of the large-signal model of the converter [given by (3)] using the time-domain technique, some simulations were carried out using Simulink toolbox in MATLAB version 8.4. The same set of converter parameter values, given by (7), was used. Fig. 3 shows the output voltage response of the converter obtained using some duty cycle disturbances. Here, at time $t = 0.35\,\text{s}$, the duty cycle was increased by $\sim$2% and at time $t = 0.55\,\text{s}$, it was restored to its nominal

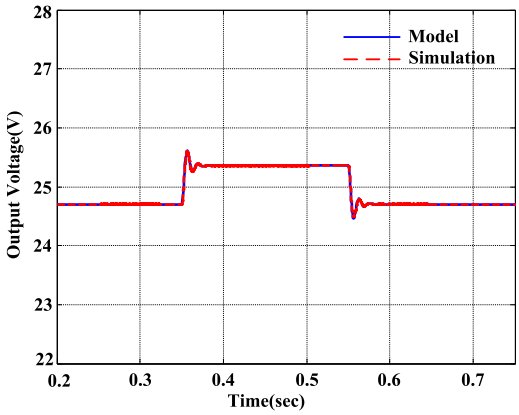

Fig. 3. Comparison of the output voltage responses for a 2% disturbance in the duty cycle.

value. The results show a good correspondence between the proposed model and the actual electrical circuit simulation of the converter. As such, the derived large-signal model can be suitably used to design an appropriate controller for the high step-up dc–dc converter.

III. Adaptive Current-Mode Controller Design

In this section, an adaptive current-mode control of a high step-up dc–dc converter is addressed. The traditional current-mode controller (of the form used in [16]–[19]) is given first to demonstrate its shortcoming when applied to systems with unknown loads.

A. Traditional Current-Mode Controller

The expression of the conventional current-mode controller is given by

$$u = U_a - K_{\mathrm{Pt}}\left(i_{L_1} - I_{L_{1a}}\right) - K_{\mathrm{It}}\int_0^t \left(v_o\left(\tau\right) - V_d\right)d\tau \quad (9)$$

where $K_{\mathrm{Pt}}(>0)$ and $K_{\mathrm{It}}(>0)$ are the controller gains and $I_{L_{1a}}$ is given by (6). This is just one form of the current-mode control in which the inductor current and output voltage are used for feedback purposes (see [16]–[19]). A voltage integral action is mainly added to reduce the steady-state error in the output voltage to a negligible value [18]. In (9), $I_{L_{1a}}$ is given by $I_{L_{1a}} = V_d(V_d+E)/2RE$ [see (6)]. For implementation purposes, $I_{L_{1a}}$ is calculated using the nominal value of the load resistance R. However, in a practical system, R may change. Also, in applications where R is unknown, (9) may not be used. To overcome these problems, the adaptive current-mode controller is proposed in the following section.

B. Adaptive Current-Mode Controller

When the load and parasitic resistances are unknown, the following control law can be used:

$$u = U_a - K_P\left(i_{L_1} - \hat{I}_{L_{1a}}\right) \quad (10)$$

where

$$\hat{I}_{L_{1a}} = \frac{V_d\left(V_d+E\right)}{2\hat{R}_a E} = \frac{V_d\left(V_d+E\right)}{2E}\hat{\theta}. \quad (11)$$

In (11), $\hat{\theta}$ is the estimate of $\theta = 1/R_a \approx 1/R$ when $r_C/R \approx 0$ and $r_{C_1}/R \approx 0$. Note that, R_a is just the approximation of R. The proposed adaptation algorithm is described by

$$\frac{d\hat{\theta}}{dt} = -\frac{2\alpha f_m e_4}{1+\alpha^2 e_4^2} \quad (12)$$

where $e_4 = v_o - V_d$, and α and f_m are user specified positive constants. Adaptive laws with normalization are used in adaptive control [25]. Let

$$f = -\frac{2\alpha f_m e_4}{1+\alpha^2 e_4^2} \quad (13)$$

then

$$\frac{df}{de_4} = -\frac{2\alpha f_m\left(1-\alpha^2 e_4^2\right)}{\left(1+\alpha^2 e_4^2\right)^2}. \quad (14)$$

Setting (14) to zero yields $e_4 = \pm 1/\alpha$ and substituting this in (12) gives $d\hat{\theta}/dt = \pm f_m$. Hence, $|d\hat{\theta}/dt| \le f_m$ for all t. This shows that the adaptation algorithm (12) has an optimized $d\hat{\theta}/dt$ and it is bounded by f_m. Moreover, (12) affords an integral action, which is necessary for the adequate operation of a practical control system.

C. Stability Analysis of the Adaptive Current-Mode Controlled System

With $r_C/R \approx 0, r_{C_1}/R \approx 0$, and $R_a \approx R$, an approximate stability analysis is performed to gain an insight into the adaptive current-mode controlled system. The following errors are defined:

$$\begin{aligned} e_1 &= i_{L_1} - I_{L_1}, \quad e_2 = v_C - V_C, \quad e_3 = v_{C_1} - V_{C_1}, \\ e_4 &= v_o - V_d, \quad \tilde{\theta} = \hat{\theta} - \theta. \end{aligned} \quad (15)$$

Now, substituting (15), (10), and (11) into (3) yields the following error dynamics:

$$\begin{aligned} \frac{de_1}{dt} \approx\ & -\frac{\beta\left(1-U_a+K_P e_1-\sigma\tilde{\theta}\right)}{2L_1}\left(e_1+I_{L_1}\right) \\ & + \frac{1-U_a+K_P e_1-\sigma\tilde{\theta}}{2L_1}\left(e_2+V_C\right) \\ & - \frac{1-U_a+K_P e_1-\sigma\tilde{\theta}}{2L_1}\left(e_3+V_{C_1}\right) \\ & + \frac{U_a-K_P e_1+\sigma\tilde{\theta}}{L_1}E \end{aligned} \quad (16)$$

$$\begin{aligned} \frac{de_2}{dt} \approx\ & -\frac{1-U_a+K_P e_1-\sigma\tilde{\theta}}{C}\left(e_1+I_{L_1}\right) \\ & - \frac{U_a-K_P e_1+\sigma\tilde{\theta}}{r_C C}\left(e_2+V_C\right) \\ & + \frac{U_a-K_P e_1+\sigma\tilde{\theta}}{r_C C}E \end{aligned} \quad (17)$$

$$\frac{de_3}{dt} \approx \frac{1-U_a+K_Pe_1-\sigma\tilde{\theta}}{2C_1}(e_1+I_{L_1}) - \frac{U_a-K_Pe_1+\sigma\tilde{\theta}}{r_{C_1}C_1}(e_3+V_{C_1}) + \frac{U_a-K_Pe_1+\sigma\tilde{\theta}}{2r_{C_1}C_1}(e_4+V_d) - \frac{U_a-K_Pe_1+\sigma\tilde{\theta}}{2r_{C_1}C_1}E \tag{18}$$

$$\frac{de_4}{dt} \approx \frac{U_a-K_Pe_1+\sigma\tilde{\theta}}{r_{C_1}C_o}(e_3+V_{C_1}) - \frac{1}{C_o}\left(\frac{1}{R}+\frac{U_a-K_Pe_1+\sigma\tilde{\theta}}{2r_{C_1}}\right)(e_4+V_d) + \frac{U_a-K_Pe_1+\sigma\tilde{\theta}}{2r_{C_1}C_o}E \tag{19}$$

$$\frac{d\tilde{\theta}}{dt} = -\frac{2\alpha f_m e_4}{1+\alpha^2 e_4^2} \tag{20}$$

where

$$\sigma = K_P\,\frac{V_d\,(V_d+E)}{2E}. \tag{21}$$

The desired equilibrium point of (16)–(20) is given by $(e_{1\infty}, e_{2\infty}, e_{3\infty}, e_{4\infty}, \tilde{\theta}_\infty) = (0,0,0,0,0)$. Considering the difficulty of proving the stability of the adaptive current-mode controlled system, an analysis based on the Lypunov indirect method is carried out [13]. Linearization of (16)–(20) about the equilibrium point given by $(e_{1\infty}, e_{2\infty}, e_{3\infty}, e_{4\infty}, \tilde{\theta}_\infty)$ and using the approximate values of I_{L_1}, V_C, and V_{C_1} yield the following linearized system of the form [26]:

$$\frac{dy}{dt} \approx Ny \tag{22}$$

where $y = [y_1\ y_2\ y_3\ y_4\ y_5]^T$, $y_1 = e_1 - e_{1\infty}$, $y_2 = e_2 - e_{2\infty}$, $y_3 = e_3 - e_{3\infty}$, $y_4 = e_4 - e_{4\infty}$, $y_5 = \tilde{\theta} - \tilde{\theta}_\infty$, and the matrix N is given in the equation at the bottom of the page.

The linearized system (22) will be stable if all the eigenvalues of N, i.e., the roots of $p_5(s) = |sI - N| = 0$, where s is a complex variable, lie in the open left half of the complex s-plane. Thus, for a given set of circuit parameters, the controller gains K_p, f_m, and α can be chosen to ensure that the real parts of the eigenvalues of N are negative. As the polynomial $p_5(s)$ is of high order, the root locus method [27] can be used to analyze the stability of the closed-loop system. In this method, any two controller parameters, say α and f_m, are kept constant and the other controller parameter, i.e., K_p is varied until the eigenvalues of *N* appear in the right half complex plane. This is done to determine the range of K_p to ensure the system stability.

The same procedure can be used to find the ranges of stability of other controller parameters such as α and f_m to ensure system stability. For illustration purpose, consider the values of the circuit parameters given by (7). The corresponding polynomial $p_5(s)$ is given by

$$\begin{aligned} p_5(s) = {} & s^5 + (7091.1K_p + 98167)\,s^4 \\ & + \left(6.96\times10^8 K_p + 2.32\times10^9\right)s^3 \\ & + \left(1.64\times10^{13}K_p - 6.63\times10^9\alpha f_m K_p \right. \\ & \left. + 3.26\times10^{11}\right)s^2 + \left(3.02\times10^{14}K_p - 5.6\times10^{13}\right. \\ & \left.\times\ \alpha f_m K_p + 6.19\times10^{14}\right)s + 8\times10^{18}\alpha f_m K_p. \end{aligned} \tag{23}$$

Fig. 4(a) shows the root locus plot of $p_5(s)$ using $\alpha = 0.25$, $f_m = 1$, and $0 \le K_p \le 5$. The arrows show how the dominant poles are moving for the increasing values of K_p. Similarly, Fig. 4(b) shows the root locus plot using $\alpha = 0.25$, $K_p = 2$, and $0 \le f_m \le 2$, whereas Fig. 4(c) shows the root locus plot for $f_m = 1$, $K_p = 2$, and $0 \le \alpha \le 0.5$. It is clear that in order to ensure system stability, there are limits to the values of K_p, α, and f_m to ensure the system stability. As such, small values of the controller parameters are to be chosen to ensure system stability. The detailed discussion on the effect of varying controller gains on the transient response of the system is given in next section.

Remark 1: If the system (22) is stable, then $y \to 0$. However, it is worth pointing out that since R_a is just the approximation of R, $\hat{\theta}$ will not tend to $1/R$, but instead it will tend to $1/R_a$.

Remark 2: Since linearization is used in this paper to analyze the system stability, the results are valid only in the neighborhood of a specific operating point. A weakness of the paper is that the proof of global stability of the proposed adaptive current-mode controlled scheme is not shown. However, it is worth noting that the semiglobal asymptotic stabilizing properties of the conventional current-mode control of the traditional dc–dc boost converter have been established [28].

$$N = \begin{bmatrix} \frac{-\beta(1-U_a)-\beta K_p I_{L_{1a}}+K_pV_{Ca}-K_pV_{C_{1a}}-2K_pE}{2L_1} & \frac{(1-U_a)}{2L_1} & -\frac{(1-U_a)}{2L_1} & 0 & \frac{\beta\sigma I_{L_{1a}}-\sigma V_{Ca}+\sigma V_{C_{1a}}+2\sigma E}{2L_1} \\ \frac{-(1-U_a)r_C-K_pr_C I_{L_{1a}}+K_pV_{Ca}-K_pE}{r_CC} & \frac{-U_a}{r_CC} & 0 & 0 & \frac{\sigma I_{L_{1a}}r_C-\sigma V_{Ca}+\sigma E}{r_CC} \\ \frac{(1-U_a)r_{C_1}+K_pr_{C_1}I_{L_{1a}}+2K_pV_{C_{1a}}-K_pV_d+K_pE}{2r_{C_1}C_1} & 0 & \frac{-U_a}{r_{C_1}C_1} & \frac{U_a}{2r_{C_1}C_1} & \frac{-\sigma I_{L_{1a}}r_{C_1}-2\sigma V_{C_{1a}}+\sigma V_d-\sigma E}{2r_{C_1}C_1} \\ \frac{-2K_pV_{C_{1a}}+K_pV_d-K_pE}{2r_{C_1}C_o} & 0 & \frac{U_a}{r_{C_1}C_o} & \frac{-U_a}{2r_{C_1}C_o}-\frac{1}{RC_o} & \frac{2\sigma V_{C_{1a}}-\sigma V_d+\sigma E}{2r_{C_1}C_o} \\ 0 & 0 & 0 & -2\alpha f_m & 0 \end{bmatrix}$$

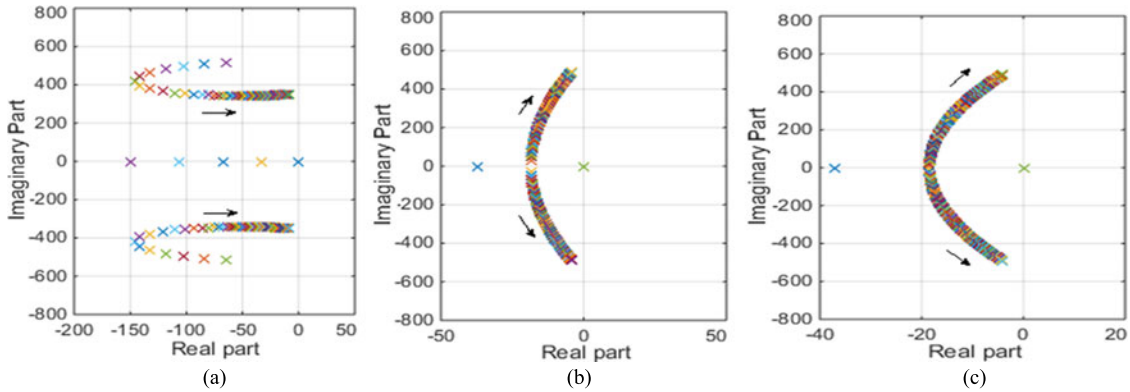

Fig. 4. Root locus plots: (a) for $\alpha = 0.25$, $f_m = 1$, and $0 \le K_p \le 5$; (b) for $\alpha = 0.25$, $K_p = 2$, and $0 \le f_m \le 2$; and (c) for $f_m = 1$, $K_p = 2$, and $0 \le \alpha \le 0.5$.

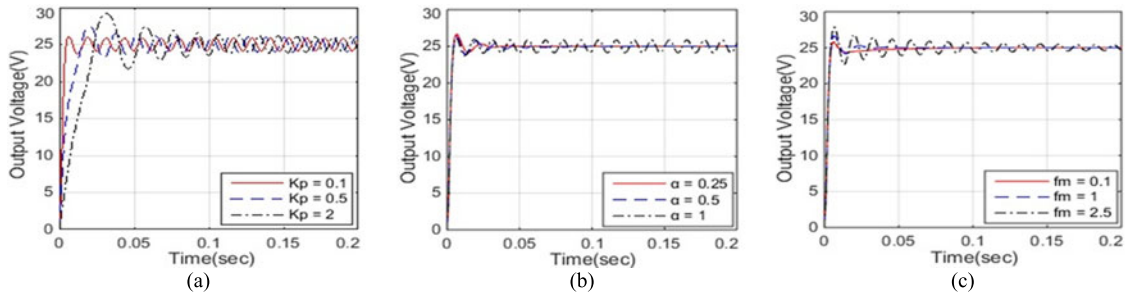

Fig. 5. Output voltage response for varying controller gains: (a) for $\alpha = 1$, $f_m = 1$, and varying K_p; (b) for $K_{\rm pa} = 0.1$, $f_m = 1$, and varying α; and (c) for $K_{\rm pa} = 0.1$, $\alpha_a = 0.25$, and varying f_m.

D. Effect of Controller Gains on the Output Response

Since there are three controller gains associated with the proposed controller given by (10)–(12), some MATLAB-based simulations were conducted to investigate their effect on the transient output response of the system. This will help the designer to select the appropriate values for the controller gains to achieve the desired output response. The same set of converter parameter values, given by (7), was used to obtain the results.

In the initial selection of K_p, α, and f_m, K_p is chosen to be "small," whereas α and f_m are set to 1. To obtain a satisfactory response, two parameters, i.e., α and f_m are kept constant, whereas the other one, i.e., K_p is fine tuned to give the "best" response. It was found that as the value of K_p increases, the overshoot and the settling time of the transient output response also increase as shown in Fig. 5(a). Thus, the appropriate small value of K_p, i.e., $K_{\rm pa}$ is initially chosen to obtain a fast output response with minimum overshoot. Next, $K_{\rm pa}$ and f_m are kept constant, whereas α is varied to achieve an improved response. As can be seen from Fig. 5(b), as the value of α increases, the oscillations in the response also increase. Thus, the controller gain α is fine tuned to its optimum value, say α_a, to obtain a smooth steady-state response with the least oscillations. Finally, once the appropriate values $K_{\rm pa}$ and α_a are obtained, the gain f_m is varied to give a further improved response. Fig. 5(c) shows the effect of the varying controller gain f_m on the output voltage response of the converter.

IV. Experimental Results

In this section, some experimental results are provided to validate the effectiveness of the proposed adaptive current-mode controller for the high step-up dc–dc converter. The performance of the proposed controller is compared with that of the traditional current-mode controller of the form used in [18]. The following set of circuit parameter values, given by (24), was used to obtain the results. Also, the switching frequency used was 10 kHz.

$$E = 3.3\,\text{V}, \quad V_d = 25\,\text{V}, \quad L_1 = L_2 = 1\,\text{mH},$$
$$C = C_1 = C_2 = C_0 = 68\,\mu\text{F}, \quad R = 2\,\text{k}\Omega. \tag{24}$$

A. Traditional Current-Mode Control

The current-mode controller (9) was first implemented to regulate the high step-up dc–dc converter [18]. For implementation purposes, a voltage feedback factor ($\beta = 1/10$) was used in (9) and the modified control law is given as follows:

$$u = U_{\rm as} - K_{\rm Pt}\left(i_{L_1} - I_{L_{1a}}\right) - K_{\rm It}\int_0^t \left(v_{\rm os}(\tau) - V_{\rm ds}\right) d\tau \tag{25}$$

where $U_{\rm as} = (V_{\rm ds} - 3E_s)/(V_{\rm ds} + E_s)$, $v_{\rm os} = \beta v_o$, $V_{\rm ds} = \beta V_d$, and $E_s = \beta E$. Fig. 6(a) shows the output voltage response and corresponding control signal for a step change in the reference voltage from $V_d = 0\,\text{V}$ to $V_d = 25\,\text{V}$ and a change in the load resistance from $R = 2\,\text{k}\Omega$ to $R = 0.667\,\text{k}\Omega$ and vice-versa.

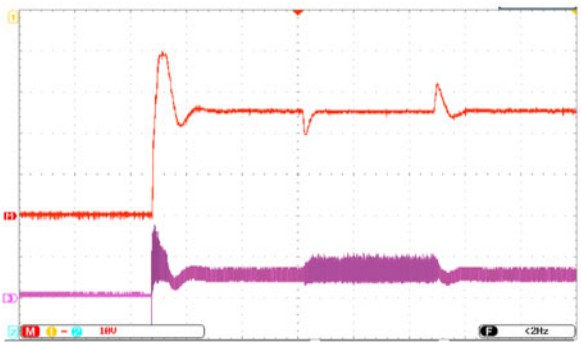

Ch. MATH (Output Voltage): 10 V/div, 1 s/div,
Ch. 3 (Control Signal): 1 V/div, 1 s/div
(a)

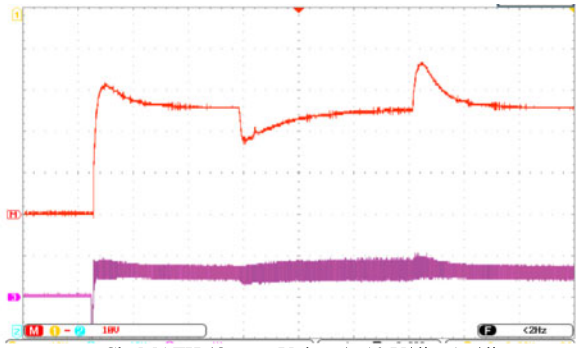

Ch. MATH (Output Voltage): 10 V/div, 1 s/div,
Ch. 3 (Control Signal): 1 V/div, 1 s/div
(b)

Fig. 6. Output voltage response and control signal obtained using the traditional current-mode controller for a step change in the reference voltage from $V_d = 0\,\mathrm{V}$ to $V_d = 25\,\mathrm{V}$, followed by a change in the load resistance from $R = 2\,\mathrm{k}\Omega$ to $R = 0.667\,\mathrm{k}\Omega$ and vice versa: (a) Using $K_{\mathrm{Pt}} = 2$ and $K_{\mathrm{It}} = 5$; and (b) Using $K_{\mathrm{Pt}} = 2$ and $K_{\mathrm{It}} = 0.5$.

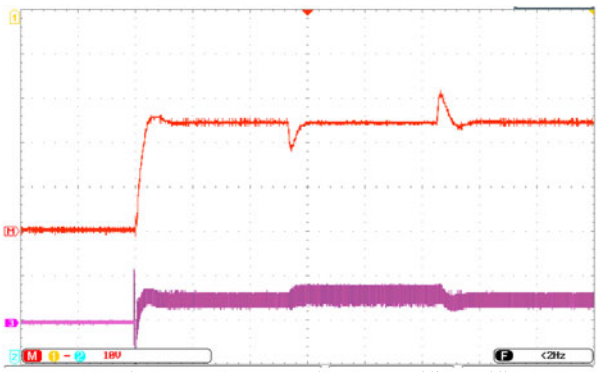

Ch. MATH (Output Voltage): 10 V/div, 1 s/div,
Ch. 3 (Control Signal): 1 V/div, 1 s/div
(a)

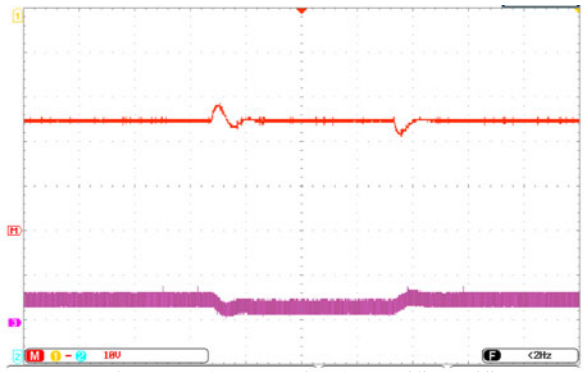

Ch. MATH (Output Voltage): 10 V/div, 1 s/div,
Ch. 3 (Control Signal): 1 V/div, 1 s/div
(b)

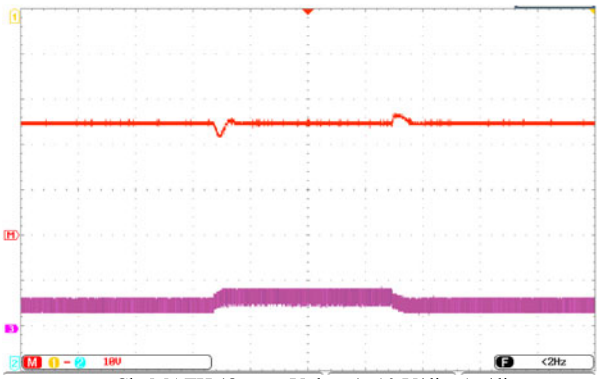

Ch. MATH (Output Voltage): 10 V/div, 1 s/div,
Ch. 3 (Control Signal): 1 V/div, 1 s/div
(c)

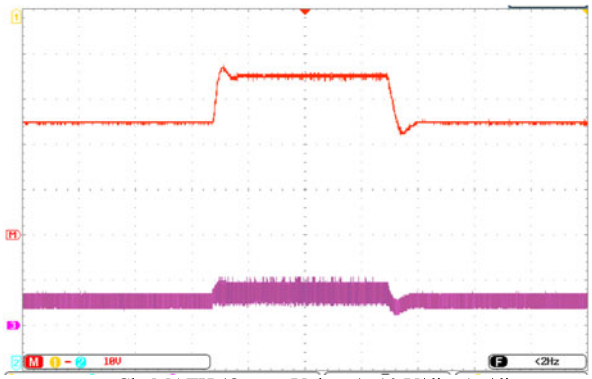

Ch. MATH (Output Voltage): 10 V/div, 1 s/div,
Ch. 3 (Control Signal): 1 V/div, 1 s/div
(d)

Fig 7. Output voltage response and control signal obtained using the adaptive current-mode controller: (a) step change in the reference voltage from $V_d = 0\,\mathrm{V}$ to $V_d = 25\,\mathrm{V}$, followed by a change in the load resistance from $R = 2\,\mathrm{k}\Omega$ to $R = 0.667\,\mathrm{k}\Omega$ (vice versa); (b) change in the load resistance from $R = 2\,\mathrm{k}\Omega$ to $R = 4\,\mathrm{k}\Omega$ and vice versa; (c) change in the input voltage from $E = 3.3\,\mathrm{V}$ to $E = 2.5\,\mathrm{V}$ and vice versa; and (d) change in the reference voltage from $V_d = 25\,\mathrm{V}$ to $V_d = 35\,\mathrm{V}$ and vice versa.

Here, $K_{\mathrm{Pt}} = 2$ and $K_{\mathrm{It}} = 5$ were used. It can be seen that even though the output voltage was rapidly restored to its desired value V_d after the onset of load disturbances, the response had a considerably large overshoot when $K_{\mathrm{It}} = 5$ was used. Fig. 6(b) shows the transient output response and the load change response of the converter obtained using $K_{\mathrm{It}} = 0.5$. It is evident that as the value of the integral gain K_{It} was decreased, the overshoot of the transient response was reduced but at the expense of an increased settling time of the load change response. Therefore, there is a tradeoff between the overshoot and

the settling time of the output response when the traditional current-mode controller of form (9) is used to regulate the high step-up dc–dc converter.

B. Adaptive Current-Mode Controller

The adaptive current-mode controller of the form (10)–(12) was next implemented using simple analog components. The division and multiplication functions were realized using the AD 633 Chip. The inductor current was measured using the Hall-effect sensor LTS-6NP from LEM. Also, in order to implement the PWM-based current-mode controller, the control signal for the switch was generated using a comparator IC LM311 and a triangular waveform of magnitude 1 $\mathrm{V_{peak-peak}}$. Moreover, for implementation purposes, a voltage feedback factor β was introduced in (10) to give

$$u = U_{\mathrm{as}} - K_P\left(i_{L_1} - \hat{I}_{L_{1\mathrm{as}}}\right) \tag{26}$$

where

$$\hat{I}_{L_{1\mathrm{as}}} = \frac{V_{\mathrm{ds}}\left(V_{\mathrm{ds}} + E_s\right)}{2E_s}\hat{\theta}_s, \quad \frac{d\hat{\theta}_s}{dt} = -\frac{2\alpha_c f_{\mathrm{mc}} e_{4s}}{1+\alpha_c^2 e_{4s}^2},$$
$$\alpha_c = \frac{\alpha}{\beta}, \quad f_{\mathrm{mc}} = \frac{f_m}{\beta}.$$

Here, $\hat{\theta}_s = \hat{\theta}/\beta$ and $e_{4s} = \beta e_4$ represent the scaled values of $\hat{\theta}$ and e_4, respectively. The scaling factor was set as $\beta = 1/10$. Also, the values of K_P, α_c, and f_{mc} used were 2, 1, and 1, respectively to achieve satisfactory responses.

Fig. 7(a) shows the transient output response and corresponding control signal for a step change in the reference voltage from $V_d = 0\,\mathrm{V}$ to $V_d = 25\ \mathrm{V}$ and a change in the load resistance from $R = 2\,\mathrm{k\Omega}$ to $R = 0.667\,\mathrm{k\Omega}$ and vice-versa. It can be seen that as compared to Fig. 6, an almost critically damped transient output response was obtained with negligible overshoot. Also, the load change response has a comparatively less worst case settling time of $\sim$0.4 s as compared to the worst case settling time of $\sim$1.2 s obtained using the current-mode controller (9). Fig. 7(b) shows the output voltage response and corresponding control signal of the converter when the load resistance R was changed from $2k\Omega$ to $4\,\mathrm{k\Omega}$ and vice versa. Next, the ability of the proposed controller to handle the input voltage as well as the reference voltage variations was investigated. Fig. 7(c) shows the output voltage response for a change in the input voltage from $E = 3.3\,\mathrm{V}$ to $E = 2.5\,\mathrm{V}$ and vice versa. The output voltage was rapidly restored to the desired V_d after the onset of the input voltage disturbances. Fig. 7(d) shows the output voltage response and the control signal when V_d was changed from 25 to 35 V and then back to 25 V. These results verify the effectiveness of the adaptive current-mode controller for the regulation of the high step-up dc-dc converter.

V. Conclusion

The modeling of the high step-up dc–dc converter and its control using an adaptive current-mode approach was addressed. The modeling took into account of the presence of some parasitic resistances in the converter circuit in order to obtain the averaged converter dynamics. The accuracy of the derived model of the converter was verified via both frequency-domain and time-domain techniques. In addition, an adaptive current-mode controller for the converter in the presence of an unknown load was proposed. As compared to the existing current-mode controller, the proposed controller has better regulation properties as borne out by the experimental results. As the structure of the proposed controller is quite generic, the control law can also be used for the regulation of other high-order dc–dc converters. Moreover, the proposed adaptive law can be combined with other state-of-the-art controllers like SMCs to improve their regulation properties.

Appendix

The generalized small-signal model of the converter is derived by linearizing (3) around the equilibrium point given by (5)–(6). If some small ac perturbations are introduced in the system about the steady-state equilibrium point, the resulting output response can be decomposed into two parts, viz., the ac terms and the dc terms. Neglecting the dc terms (since their derivative are zero) and focusing on the ac behavior, a small-signal linear model of the high step-up dc–dc converter can be obtained as

$$\dot{\tilde{x}} = a\tilde{x} + b\tilde{u} \tag{A1}$$
$$\tilde{y} = c\tilde{x} \tag{A2}$$

where $\tilde{u}$ represents the small signal variations in the duty cycle u, i.e., $u = U_a + \tilde{u}$ and $\tilde{x}$ represents the small signal variations in the state variables such that $\tilde{x} = [\tilde{i}_{L_1}\ \tilde{v}_C\ \tilde{v}_{C_1}\ \tilde{v}_o\ ]^T$. Also, $\tilde{y} = [\tilde{v}_o\ ]$ denotes the small signal variations in the output. Matrices a, b, and c are given by

$$a = \begin{bmatrix} -\frac{\beta(1-U_a)}{2L_1} & \frac{1-U_a}{2L_1} & -\frac{1-U_a}{2L_1} & 0 \\ -\frac{1-U_a}{C} & -\frac{U_a}{r_C C} & 0 & 0 \\ \frac{1-U_a}{2C_1} & 0 & -\frac{U_a}{r_{C_1} C_1} & \frac{U_a}{2r_{C_1} C_1} \\ 0 & 0 & \frac{U_a}{r_{C_1} C_o} & -\frac{U_a}{2r_{C_1} C_o} \end{bmatrix},$$

$$b = \begin{bmatrix} \frac{1}{2L_1}\left(\beta I_{L_{1a}} - V_{\mathrm{Ca}} + V_{C_{1a}} + 2E\right) \\ \frac{1}{r_C C}\left(r_C I_{L_{1a}} - V_{\mathrm{Ca}} + E\right) \\ \frac{1}{2r_{C_1} C_1}\left(-r_{C_1} I_{L_{1a}} - 2V_{C_{1a}} + V_d - E\right) \\ \frac{1}{2r_{C_1} C_1}\left(2V_{C_{1a}} - V_d + E\right) \end{bmatrix}, \text{and}$$

$$c^T = \begin{bmatrix} 0\,0\,0\,1 \end{bmatrix}. \tag{A3}$$

The control-to-output transfer function of the converter can now be easily obtained by applying the Laplace transform to (A1) and (A2) and using the zero initial conditions. The transfer function is given by

$$\frac{\tilde{v}_0(s)}{\tilde{u}(s)} = c(sI - a)^{-1}b \tag{A4}$$

ACKNOWLEDGMENT

The authors would like to acknowledge the contribution of Mr. Tan Yong Qi Kelvin for his assistance in developing the experimental prototype and carrying out the experiments.

REFERENCES

[1] G. Wu, X. Ruan, and Z. Ye, "Non-isolated high step-up DC–DC converters adopting switched-capacitor cell," *IEEE Trans. Ind. Electron.*, vol. 62, no. 1, pp. 383–393, Jan. 2015.

[2] W. H. Li and X. N. He, "Review of nonisolated high-step-up DC–DC converters in photovoltaic grid-connected applications," *IEEE Trans. Power Electron.*, vol. 58, no. 4, pp. 1239–1250, Apr. 2011.

[3] F. Guo, C. Wen, J. Mao, and Y.-D. Song, "Distributed secondary voltage and frequency restoration control of droop-controlled inverter-based microgrids," *IEEE Trans. Ind. Electron.*, vol. 62, no. 7, pp. 4355–4364, Jul. 2015.

[4] A. J. Sabzali, E. H. Ismail, and H. M. Behbehani, "High voltage step-up integrated double Boost-Sepic DC–DC converter for fuel-cell and photovoltaic applications," *Renewable Energy*, vol. 82, pp. 44–53, 2015.

[5] G. R. Walker and P. C. Sernia, "Cascaded DC–DC converter connection of photovoltaic modules," *IEEE Trans. Power Electron.*, vol. 19, no. 4, pp. 1130–1139, Jul. 2004.

[6] A. A. Fardoun and E. H. Ismail, "Ultra step-up DC–DC converter with reduced switch stress," *IEEE Trans. Ind. Appl.*, vol. 46, no. 5, pp. 2025–2034, Sep./Oct. 2010.

[7] T. J. Liang, S. M. Chen, L. S. Yang, J. F. Chen, and A. Ioinovici, "Ultralarge gain step-up switched-capacitor DC–DC converter with coupled inductor for alternative sources of energy," *IEEE Trans. Circuits Syst. I, Reg. Papers*, vol. 59, no. 4, pp. 864–874, Apr. 2012.

[8] J. Zeng, W. Qiao, and L. Qu, "A single-switch LCL-resonant isolated DC–DC converter," in *Proc. IEEE Energy Convers. Congr. Expo.*, Sep. 2013, pp. 5496–5502.

[9] F. L. Luo and H. Ye, *Advanced DC/DC Converters*. Boca Raton, FL, USA: CRC Press, 2003.

[10] M. Prudente, L. L. Pfitscher, G. Emmendoerfer, E. F. Romanelli, and R. Gules, "Voltage multiplier cells applied to non-isolated DC–DC converters," *IEEE Trans. Power Electron.*, vol. 23, no. 2, pp. 871–887, Mar. 2008.

[11] B. Axelrod, Y. Berkovich, and A. Ioinovici, "Switched capacitor/switched-inductor structures for getting transformerless hybrid DC–DC PWM converters," *IEEE Trans. Circuits Syst. I, Reg. Papers*, vol. 55, no. 2, pp. 687–696, Mar. 2008.

[12] J. C. Rosas-Caro, J. M. Ramirez, and P. M. Garcia-Vite, "Novel DC–DC multilevel boost converter," in *Proc. IEEE Power Electron. Spec. Conf.*, 2008, pp. 2146–2151.

[13] O. Lopez-Santos, L. Martinez-Salamero, G. Garcia, H. Valderrama-Blavi, and T. Sierra-Polanco, "Robust sliding-mode control design for a voltage regulated quadratic boost converter," *IEEE Trans. Power Electron.*, vol. 30, no. 4, pp. 2313–2327, Apr. 2015.

[14] M. G. Ortiz-Lopez, J. Leyva-Ramos, E. E. Carbajal-Gutierrez, and J. A. Morales-Saladana, "Modelling and analysis of switch-mode cascade converters with single active switch," *IET Power Electron.*, vol. 1, no. 4, pp. 478–487, 2008.

[15] F. H. Dupont, C. Rech, R. Gules, and J. R. Pinheiro, "Reduced-order model and control approach for the boost converter with a voltage multiplier cell," *IEEE Trans. Power Electron.*, vol. 28, no. 7, pp. 3395–3404, Jul. 2013.

[16] I. Cervantes, D. Garcia, and D. Noriega, "Linear multiloop control of quasi-resonant converters," *IEEE Trans. Power Electron.*, vol. 18, no. 5, pp. 1194–1201, Sep. 2003.

[17] C. Y. Chan, "A nonlinear control for dc–dc power converters," *IEEE Trans. Power Electron.*, vol. 22, no. 1, pp. 216–222, Jan. 2007.

[18] C. Y. Chan, "Comparative study of current-mode controllers for a high-order boost dc–dc converter," *IET Power Electron.*, vol. 7, no. 1, pp. 237–243, 2014.

[19] S. H. Chincholkar and C. Y. Chan, "Investigation of current-mode controlled cascade boost converter systems: Dynamics and stability issues," *IET Power Electron.*, vol. 9, no. 5, pp. 911–920, 2016.

[20] O. Lopez-Santos, L. Martinez-Salamero, G. Garcia, H. Valderrama-Blavi, and D. O. Mercuri, "Efficiency analysis of a sliding-mode controlled quadratic boost converter," *IET Power Electron.*, vol. 6, no. 2, pp. 364–373, 2013.

[21] S. C. Tan, Y. M. Lai, and C. K. Tse, "A unified approach to the design of PWM-based sliding-mode voltage controller for basic DC–DC converters in continuous conduction mode," *IEEE Trans. Circuits Syst. I, Reg. Papers*, vol. 53, no. 8, pp. 1816–1827, Aug. 2006.

[22] S. C. Tan, Y. M. Lai, and C. K. Tse, "Indirect sliding mode control of power converters via double integral sliding surface," *IEEE Trans. Power Electron.*, vol. 23, no. 2, pp. 600–611, Mar. 2008.

[23] S.-C. Tan and Y. M. Lai, "Constant-frequency reduced-state sliding-mode current controller for Cuk converters," *IET Power Electron.*, vol. 1, no. 4, pp. 466–477, Dec. 2008.

[24] S. Baacha, L. Munteanu, and A. Luliana Bratcu, *Power Electronics Converters Modeling and Control: With Case Studies*. London: Springer-Verlag, 2014.

[25] P. A. Ioannou, and J. Sun, *Robust Adaptive Control*, Upper Saddle River, NJ: Prentice-Hall, 1996.

[26] H. Khalil, *Nonlinear Systems*, 3rd ed. Upper Saddle River, NJ, USA: Pearson, 2000.

[27] K. Ogata, *Modern Control Engineering*, 3rd ed. Upper Saddle River, NJ, USA: Prentice-Hall, 1997.

[28] A. Ramirez and E. Perez, "Stability of current-mode control of DC–DC power converters," *Syst. Control Lett.*, vol. 45, pp. 113–119, 2002.

Chok-You Chan received the B.E., M.E., and Ph.D. degrees in electrical and electronic engineering from the University of Canterbury, Christchurch, New Zealand in 1983, 1985, and 1987, respectively.

He is currently an Associate Professor in the School of Electrical and Electronic Engineering, Nanyang Technological University, Singapore. His current research focuses on the area of converter control.

Satyajit Hemant Chincholkar received the B.Tech. degree in instrumentation and control engineering from the College of Engineering, Pune, India, in 2010. He is currently working toward the Ph.D. degree in electrical and electronic engineering at the Nanyang Technological University, Singapore.

His research interests include modeling and control of power electronic converters, simulation, and hardware.

Wentao Jiang received the B.Eng. degree in electrical engineering from Xi'an University of Technology, Xi'an, China, and the M.S. degree in electrical engineering from the National University of Singapore, Singapore, in 2011 and 2013, respectively. He is currently working toward the Ph.D. degree in electrical and electronic engineering at the Nanyang Technological University, Singapore.

His current research focuses on modeling and control of the high-order dc-dc power converters.